Talanta 86 (2011) 408–414

Contents lists available at SciVerse ScienceDirect

Talanta

journal homepage: www.elsevier.com/locate/talanta

Dye-functional mesoporous silica material for fluorimetric detection of Cr(III) in aqueous solution and biological imaging in living systems

Qingtao Meng[a], Weiping Su[a], Xiaoming Hang[b,1], Xuezhao Li[a], Cheng He[a], Chunying Duan[a,*]

[a] State Key Laboratory of Fine Chemicals, Dalian University of Technology, 2 Linggong Road, Dalian High-Tech Industrial Zone, 116024, China
[b] Institute of Environmental Systems Biology, Dalian Maritime University, Dalian 116026, China

ARTICLE INFO

Article history:
Received 5 July 2011
Received in revised form
17 September 2011
Accepted 21 September 2011
Available online 29 September 2011

Keywords:
Dye-functional mesoporous silica material
Chromium
Absorbent
Fluorescence bio-imaging

ABSTRACT

A dye-functionalized silica nanomaterial, SBA-RT was prepared by the immobilization of the Rhodamine-based chemosensor R6G-TETA within the channels of SBA-15. SBA-RT exhibits several different properties compared to the free R6G-TETA, such as higher selectivity, blue-shift of the UV–vis spectra due to special spatial environment in the channels of the mesoporous material. It presents Cr(III)-selective fluorimetric and colorimetric responses in aqueous solution. The fluorescence responses are reversible by treating with EDTA and do not vary over a broad pH range suitable for Cr(III) bioimaging application. Through isolating of the metal ions within the mesopores of the silica, SBA-RT can extract Cr(III) from the solution with only trace amounts remaining. The fluorescence images experiment demonstrated the possibility of further application in monitoring Cr(III) in living cells and organisms.

1. Introduction

Recently, inorganic host materials have been widely used as support to design functional materials used in catalysis [1–4], and drug delivery fields [5–9]. Specially, mesoporous silica materials have attracted much attention for optical applications due to their excellent properties, such as high surface area, uniform porosity, optical transparency in the UV/vis range, favorable biocompatibility and mechanical robustness [10–17]. The solid chemosensors could be achieved by covalent grafting of fluorescent receptors onto the inner surface of mesoporous silica materials [18–20]. Recently, functionalized mesoporous materials have been also used as adsorbent for wastewater containing heavy metal ions by atomic absorption spectrometry and infrared spectrophotometry [21–23]. However, these analysis methods have the following disadvantages: complicated operation, expensive instruments, unsuitable for real-time detection, etc. It is still a challenge to develop novel multifunctional materials that can detect and adsorb heavy-transition metal (HTM) ions with visualized output signals (fluorescence or color responses, etc.).

Trivalent chromium, has great impact on the metabolism of carbohydrates, fats, proteins and nucleic acids based on modulation of the action of insulin through glucose tolerance factors (GTF) [24,25]. The appropriate chromium intake is 50–200 μg per day and its deficiency causes disturbances in glucose levels and lipid metabolism. However, exposure to high levels of Cr(III) can negatively affect cellular structures [26–29]. On the other hand, chromium is an environmental pollutant and its build-up due to various industrial and agricultural activities is a matter of concern [30]. Thus, there is an urgent need to study suitable methods capable of sensing of Cr(III) in biological and environmental system [31]. However, the development of Cr(III)-specific chemosensors for quantificational detection of Cr(III) by fluorimetric methods is still a big challenge due to the lack of selective multi-chelating ligands [32,33]. Cr(III) is also one of the most effective fluorescent quenchers known due to its paramagnetic nature which also makes it difficult to develop "turn-on" types of chemosensors [34,26]. Rhodamine framework is an ideal mode to construct OFF–ON fluorescent sensors due to its particular structural property (the equilibrium between the non-fluorescent spiro-cyclic form and the highly fluorescent ring-open form) [35,36]. Of these Rhodamine-based Cr(III) fluorescent sensors have been developed [37–40], R6G-TETA is one of the most sensitive probes that exhibits excellent selectivity towards Cr(III) in HEPES aqueous solution over other transitions metal ions [41]. Upon the addition of 5 equiv. of Cr(III), about 60-fold fluorescence enhancement of R6G-TETA at 552 nm was observed. However, whether the sensor can be applied in bioimaging was not further investigated.

Bearing this in mind, we chose the Cr(III)-specific fluorescent chemosensor R6G-TETA as molecular probe and immobilized it onto the inner surface of SBA-15. We envisioned that the

* Corresponding author. Tel.: +86 411 84986261.
E-mail address: cyduan@dlut.edu.cn (C. Duan).
[1] Tel.: +86 411 84723633x821; fax: +86 411 84725675.

0039-9140/$ – see front matter © 2011 Elsevier B.V. All rights reserved.
doi:10.1016/j.talanta.2011.09.036

combination of the fluorescence sensor and mesoporous material would generate a novel multifunctional material, which could take on specific fluorescence response and high adsorptivity for Cr(III) in water. The favorable biocompatibility of the mesoporous silica material is beneficial to utilize the hybrid material in living cells and *in vivo* to study the toxicity or bioactivity of Cr(III) in living organisms.

2. Experimental

2.1. Reagents and chemicals

All reagents and solvents were of AR grade and used without further purification unless otherwise noted. SBA-15 was purchased from Jilin University High Technology Co. Ltd., 3-(triethoxysilyl)propylisocyanate was obtained from Aldrich. Triethylenetetramine and metal salts were provided by Shanghai Chemical Reagent Co., Ltd. (China). Stock solution (2×10^{-2} M) of the aqueous nitrate salts of K^+, Na^+, Ca^{2+}, Mg^{2+}, Co^{2+}, Ba^{2+}, Ni^{2+}, Zn^{2+}, Cd^{2+}, Pb^{2+}, Hg^{2+}, Cu^{2+}, Al^{3+}, Fe^{3+} and Cr^{3+} were prepared for further experiments.

2.2. Instruments and spectroscopic measurements

^{1}H NMR was measured on a Varian INOVA 400 M spectrometer with chemical shifts reported as ppm ($CDCl_3$, TMS as internal standard). X-ray powder diffraction (XRD) patterns of the SBA-15, SBA-RT were recorded on a Rigaku D/max-2400 X-ray powder diffractometer (Japan) using Cu Kα (λ = 1.5405 Å) radiation. Transmission Electron Microscope (TEM) images were taken on a Hitachi H-9000 NAR transmission electron microscope under a working voltage of 300 kV. FT-IR spectra were recorded on a Nicolet Magna-IR 750 spectrometer equipped with a Nic-Plan Microscope. UV–vis diffuse reflectance spectra were taken on a Shimadzu UV-2401PC spectrophotometer using $BaSO_4$ as the reference. Elemental analyses (C, H, and N) were performed on an Elementary Vario EL analyzer. The nitrogen adsorption and desorption isotherms were measured at 77 K using an ASAP 2010 analyzer (Micromeritics Co. Ltd.). Surface areas were calculated by the Brunauer–Emmett–Teller (BET) method, and the pore volume and pore size distributions were calculated using the Barret–Joyner–Halenda (BJH) model. Fluorescence spectra of the solution were obtained using the FS920 spectrometer (Edinburgh Instruments). Both excitation and emission slit widths were 6 nm. Fluorescence measurements were carried out in a 2 cm quartzcuvette with stirring the suspension of SBA-RT. The adsorption ability of SBA-RT for Cr(III) in water was measured by inductively coupled plasma spectrometer (Perkin Elmer). HeLa Cells and zebrafish were imaged by Nikon eclipse TE2000-5 inverted fluorescence microscopy.

2.3. Synthesis of R6G-TETA

Compound R6G-TETA was prepared according to reported procedures [41]. ^{1}H NMR ($CDCl_3$, 400 MHz) δ = 7.92 (d, 1 H), 7.45 (t, 2 H), 7.043 (t, 1 H), 6.34 (s, 2 H), 6.21 (s, 2 H), 3.52 (t, 2 H), 3.22 (t, 4 H), 2.76 (m, 2 H), 2.61 (t, 2 H), 2.51 (m, 2 H), 2.35 (m, 4 H), 1.89 (s, 6 H), 1.32 (t, 6 H).

2.4. Synthesis of SBA-IPTES

3-(Triethoxysilyl)propylisocyanate (IPTES) (0.247 g, 1 mmol) and SBA-15 (1.0 g) were suspended in anhydrous toluene (50 mL) and stirred in reflux condition under N_2 for 24 h. The precipitate formed was filtered, and adequately washed several times with toluene and CH_2Cl_2 to rinse away any surplus IPTES. A white powder was obtained and denoted as SBA-IPTES. Elemental analysis, Found: N, 2.309, C, 9.8, H 2.05. IR (KBr): ν = 3434 (vs; O–H), 2920 (w; C–H), 1636 (s; O–H), 1471 (w; –C=C–H), 1089 (vs; Si–O–Si), 798 (w; SiO–Si), 465 (m; Si–O).

2.5. Synthesis of SBA-RT

R6G-TETA (0.272 g, 0.5 mmol) and SBA-IPTES (1.0 g) were suspended in anhydrous toluene (50 mL) and stirred in reflux condition under N_2 for 24 h. The precipitate formed was filtered, and adequately washed several times with toluene and CH_2Cl_2 to rinse away any surplus R6G-TETA. A faint pink power was obtained and denoted as SBA-RT. Elemental analysis, Found: N, 2.878, C, 13.2, H 2.077. IR (KBr): ν = 3436 (vs; O–H), 2950 (w; C–H), 2830 (w; C–H), 1520 (s; –C=C–H), 1440 (w; –C=C–H), 1090 (vs; Si–O–Si), 809 (w; SiO–Si), 464 (m; Si–O).

2.6. Adsorption ability of SBA-RT for Cr(III)

SBA-RT (20 mg) and SBA-15 (20 mg) were added to the about 0.2 ppm Cr(III) solution (50 mL), respectively. The mixture was stirred for 4 h. After filtration, the concentration of residual Cr(III) in the filtrate was analyzed by inductively coupled plasma source mass spectrometer (ICP).

2.7. Imaging of HeLa cells incubated with SBA-RT and Cr(III)

HeLa cells were incubated with SBA-RT (1 ppm, suspended in PBS medium) for 30 min at 28 °C. After washing with saline to remove the remaining SBA-RT, HeLa cells were further incubated with 0.2 mM Cr(III) for another 30 min at 28 °C. HeLa cells were imaged by fluorescence microscopy.

2.8. Imaging of zebrafish incubated with SBA-RT and Cr(III)

Zebrafish was kept at 28 °C. For mating, male and female zebrafish was maintained in one tank at on a 12 h light/12 h dark cycle and then the spawning of eggs was triggered by giving light stimulation in the morning. Almost all the eggs were fertilized immediately. The 5-day old zebrafish was maintained in E3 embryo media (15 mM NaCl, 0.5 mM KCl, 1 mM $MgSO_4$, 1 mM $CaCl_2$, 0.15 mM KH_2PO_4, 0.05 mM Na_2HPO_4, 0.7 mM $NaHCO_3$, 10^{-5}% methylene blue; pH = 7.5). The 5-day old zebrafish was incubated with SBA-RT (4 ppm) in PBS media for 0.5 h at 28 °C. After washing with saline to remove the residual nanoparticles, the zebrafish was further incubated with 0.2 mM Cr(III) for another 30 min at 28 °C. Zebrafish was imaged by fluorescence microscopy.

3. Results and discussion

3.1. Synthesis and characterization of SBA-RT

Compound R6G-TETA was prepared according to the reported procedures. Intermediate material SBA-IPTES was easily synthesized by condensation of 3-(triethoxysilyl)propylisocyanate with SBA-15 in toluene [42]. SBA-RT was obtained by coupling of R6G-TETA with SBA-IPTES in toluene (Scheme 1) and characterized by elemental analysis (EA), XRD, and several spectroscopic methods.

Fig. 1 displays the FTIR spectra of SBA-15 and SBA-RT, new bands centered at around 3000–2800 cm^{-1} and 1500–1400 cm^{-1} were attributed to the C–H stretching and the aromatic stretching vibrations of Rhodamine group attached onto SBA-15, respectively [43]. The content of incorporated R6G-TETA receptor was determined by thermogravimetric analysis (TGA). As shown in Fig. 2, a slight weight loss (about 3.1%) of SBA-IPTES in the temperature

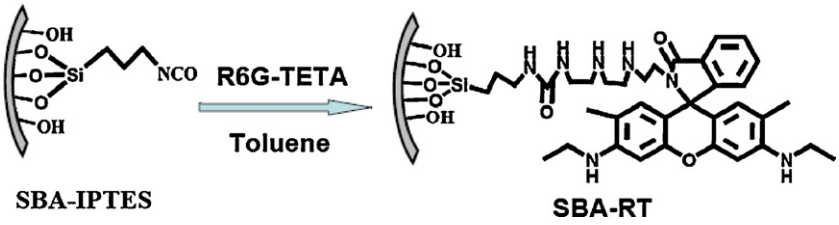

Scheme 1. Synthesis procedure of the functional material SBA-RT.

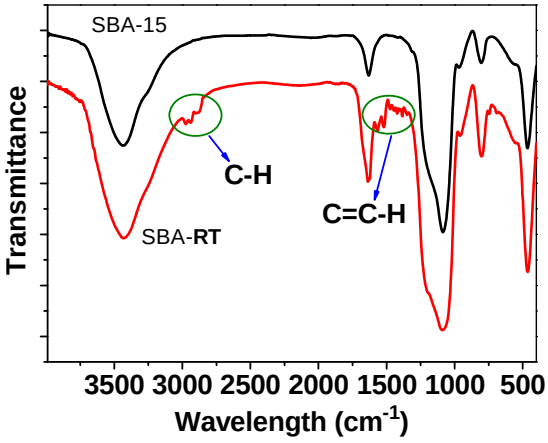

Fig. 1. FT-IR spectra of SBA-15 and SBA-RT.

range of 50–150 °C mainly due to the thermal removal of physically adsorbed water. The major weight loss (about 8.9%) event in the temperature range of 150–800 °C could be due to the thermal decomposition of IPTES. Analogously, two steps weight loss (3.3% weight loss in 50–150 °C, and 23.3% weight loss in 150–800 °C) of SBA-RT could be attributed to the removal of water and then thermal decomposition of R6G-TETA receptor, respectively [44]. Referring to elemental analysis (EA) results, we calculated that SBA-RT contains approximately 20 wt% of R6G-TETA. Accordingly, 5 ppm SBA-RT suspension corresponding to the concentration of R6G-TETA was about 1.5 μM.

The maintenance of the uniform mesopore structure of SBA-15 during the grafting process was also investigated. As shown in Fig. 3, both the isotherms of SBA-15 and SBA-RT were of type IV as defined by IUPAC, characteristic of mesoporous material with a highly uniform size distribution. However, the Brunauer–Emmett–Teller (BET) surface area of SBA-RT declined from 571 m^2/g to 385.8 m^2/g due to the linkage of R6G-TETA. Likewise, the pore volume shrinked to 0.618 cm^3/g from 0.912 cm^3/g for the parent materials. Furthermore, the Barret–Joyner–Halenda (BJH) pore diameters distribution of SBA-RT showed a decrease in diameter by 2.9 nm compared with that of SBA-15 (Fig. 3) [45]. These results demonstrated that the mesoporous structure of SBA-15 was maintained after attachment of R6G-TETA. TEM micrographs of the SBA-RT also indicated that the channel structure of SBA-15 is not destroyed by incorporation of Cr(III) probes (Fig. 4) [46].

3.2. The detection and adsorption ability of SBA-RT for Cr(III) in water

The detection ability of the functional material to Cr(III) was investigated by means of fluorescence titration. The colorless suspension of SBA-RT (5 ppm, pH = 6.4) showed very weak fluorescence due to the predominant ring-closed spirolactone [47]. Upon addition of Cr(III), the suspension showed strong fluorescence with an approximately 8-fold enhancement in the intensity (Fig. 5(a)). In addition, the Cr(III)-loaded SBA-RT after isolation from the aqueous suspension under-went a color change from almost colorless to pink (Fig. 5(a), insert). To the best of our knowledge, this is the first successful Cr(III) detection application of functional mesoporous materials by spectroscopic and "naked-eye" methods in water. While Cr(III) is more stable under acidic condition because of strong hydrolysis efficiency in water, and Rhodamine dye is usually disturbed by the proton in the detection of metal ions due to the ring-opening under acidic conditions [48]. The pH-dependence titration of SBA-RT upon addition of Cr(III) revealed that the luminescence did not vary over a pH range from 5.5 to 7.5. We also investigated the accuracy of SBA-RT by ICP spectrometric. As shown in Fig. 5(b), the fluorescence intensity increased in a linear

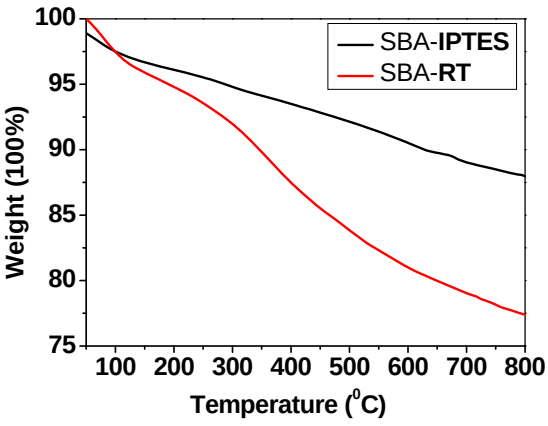

Fig. 2. TGA curves of SBA-IPTES and SBA-RT. (For interpretation of the references to color in this figure legend, the reader is referred to the web version of the article.)

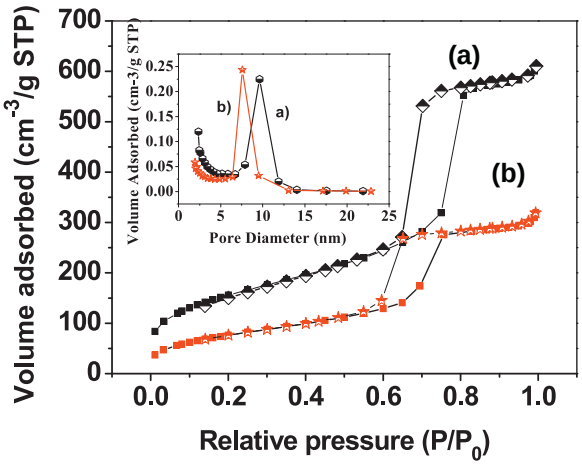

Fig. 3. Nitrogen adsorption–desorption isotherms of (a) SBA-15 and (b) SBA-RT. Inset: corresponding pore size distribution for (a) SBA-15 and (b) SBA-RT.

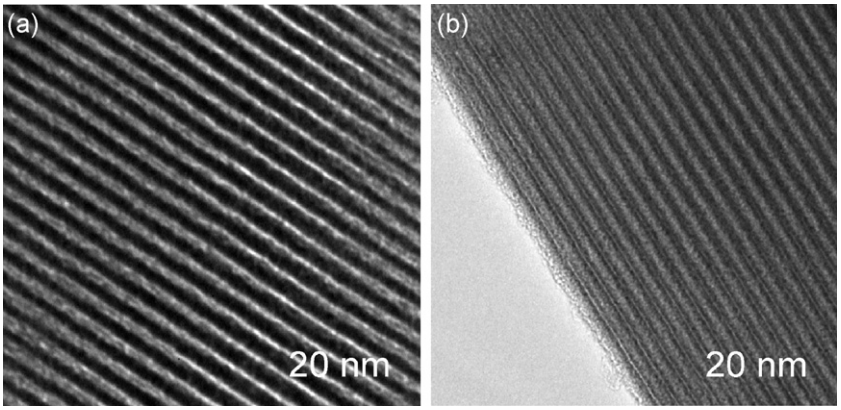

Fig. 4. TEM images of (a) SBA-15 and (b) SBA-RT.

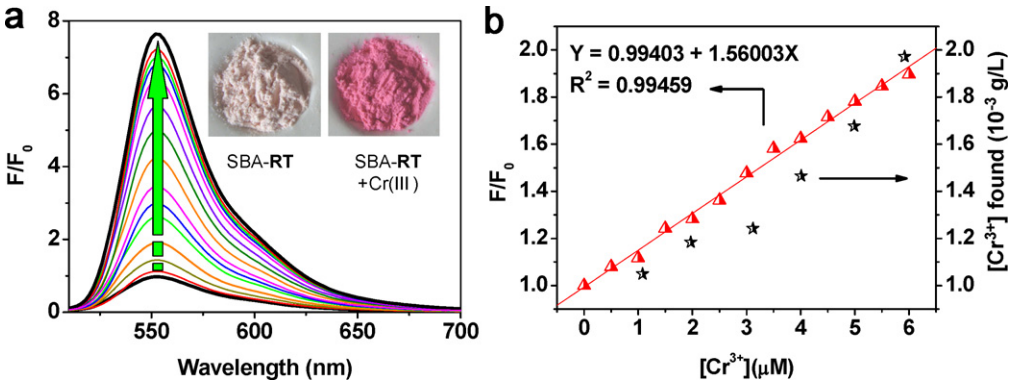

Fig. 5. (a) Fluorescence spectra of SBA-RT (5 ppm, pH = 6.4) upon addition of various amounts of Cr(III) (0–20 μM) in water. Insert: color changes for isolated SBA-RT with Cr(III). (b) Red trigons: fluorescence titration profile of the of SBA-RT (5 ppm, pH = 6.4) upon addition of Cr(III) (0–0.6 μM) in water. Black stars: the concentration of the added Cr(III) determined by ICP measurement. Emission record at 553 nm, excited at 500 nm. (For interpretation of the references to color in this figure legend, the reader is referred to the web version of the article.)

manner with the increase of the concentration of Cr(III) in the range of 0–6 μM (linearly dependent coefficient: R^2 = 0.9946), indicating the detection limit of Cr(III) by this method is 1 μM. Therefore, we believe that SBA-RT was capable of distinguishing safe and toxic levels of Cr(III) in surface water according to the 2.5 μM (0.13 ppm) China EPA (Environmental Protection Agency) standard [49]. By comparing with the ICP spectrometric measurements, the proposed chemosensor SBA-RT showed satisfactory result with lower detection limit and linear dependence at lower concentration of Cr(III) [50].

Although R6G-TETA has been successfully applied to detect Cr(III) in aqueous system, its use in related analytical techniques in the homogeneous phase is not appropriating for the separation, removal, and enrichment of Cr(III) in potential environmental application. As a solid probe, SBA-RT was insoluble in water or other common organic solvents, providing the possibility to remove the Cr(III) from the pollutant solution in heterogeneous phases. Consequently, we investigated the adsorption ability of SBA-RT to Cr(III) in water. A Cr(III) solution of about 0.2 ppm was treated with SBA-RT, after filtration, the concentration of Cr(III) solution before and after treating with SBA-RT was estimated by inductively coupled plasma source mass spectrometer (ICP). We observed that the hybrid material adsorbed almost 90% of Cr(III), and the concentration of Cr(III) remained in the solution was about 20 ppb. Whereas, the concentration of Cr(III) remained in the solution in case of SBA-15 used was 0.18 ppm. SBA-RT thus is a promising remediation material used for removing of metal ions in drinking water.

The functional nanomaterial features excellent selectivity towards Cr(III) over the other competitive cations species such as Al^{3+}, Cu^{2+}, Hg^{2+}, Zn^{2+}, Cd^{2+}, Pb^{2+}, Ni^{2+}, Co^{2+}, Ba^{2+}, Mg^{2+}, Ca^{2+}, Na^{+} and K^{+} in water. All fluorescence spectra were recorded at 553 nm within 3 min after addition of metal ions (20 μM) in the suspension of SBA-RT (5 ppm, pH = 6.4). The fluorescence emission changes of SBA-RT upon addition of various metal ions are illustrated in Fig. 6. No significant spectral changes of the suspension solution occurred in the presence of alkali or alkaline, earth metals and the first-row transition metals, such as, Fe^{3+}, Hg^{2+}, Cu^{2+}, Zn^{2+}, Cd^{2+}, Pb^{2+}, Mn^{2+}, Ni^{2+}, Co^{2+}, and Mg^{2+}, Ca^{2+}, Ba^{2+}, Na^{+}, K^{+}. However, the addition of Cr(III) ions into the suspension of SBA-RT produced an obvious fluorescence enhancement. Upon addition of Cr(III) to the above suspensions gave rise to drastic increase of their fluorescence intensities, revealing that Cr(III) has specific effects on the fluorescence responses, and the Cr(III)-specific

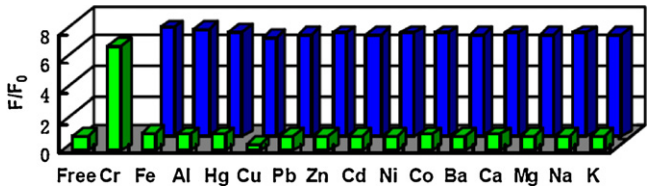

Fig. 6. Normalized fluorescence responses of SBA-RT (5 ppm, pH = 6.4) to various cations in water. The green bars represent the emission intensities of SBA-RT in the presence of cations of interest (all are 20 μM). The blue gray bars represent the change of the emission that occurs upon the subsequent addition of 20 μM of Cr(III) to the above suspension. The intensities were recorded at 553 nm, excitation at 500 nm. (For interpretation of the references to color in this figure legend, the reader is referred to the web version of the article.)

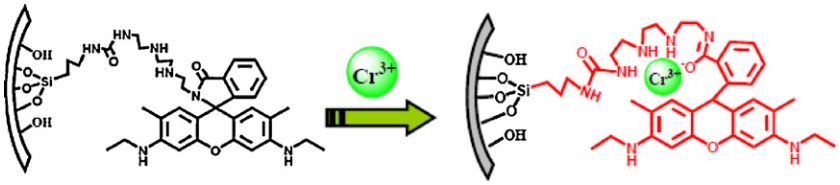

Scheme 2. Proposed binding mode of SBA-RT with Cr (III).

response was not disturbed by the competitive ions. From a view of mechanistic, Cr(III) featured optimal coordination ability to the R6G-TETA among these metal ions. Due to the small size, Cr(III) can be coordinated by one amide group, one urea group and two nitrogen atoms of the anchored rhodamine derivative in SBA-RT to form a 1:1 stable complexation species (Scheme 2). Whereas for other transition metal with larger size, it is difficult to form stable complexation species in the same coordination geometry, hardly "turn-on" the luminescence by opening the spirolactam ring of the Rhodamine. It should be noted that the detection towards Cr(III) of the free R6G-TETA was disturbed by Fe (III), while the selectivity of SBA-RT towards Cr(III) was significant improved. This phenomenon has also been reported for functional hybrid materials [51]. The quantum efficiency of SBA-RT could be increased due to the presence of silanol groups on the channels surface of SBA-15, which partly inhibits the proton transfer and influenced the coordination environment of R6G-TETA by the synergistic effect. Consequently, the Fe(III) complex with SBA-RT gives rise to less fluorescence enhancement than the Fe(III) complex with R6G-TETA, and a Cr(III)-specific fluorescence response spontaneously achieved.

UV–vis diffuse reflectance spectra were measured to further investigate the binding efficiency of SBA-RT to Cr(III). As shown in Fig. 7, once Cr(III) loaded to the hybrid material, the weak band at about 530 nm attributed to the typical absorption of Rhodamine increased obviously, indicating that the Cr(III) was efficiently bound to the receptor R6G-TETA that attached to the SBA-RT and the opening forms of the Rhodamine framework appeared [52]. However, the band position showed a blue shift of about 13 nm compared to that of R6G-TETA. A similar blue-shift phenomenon was also reported in the previous examples and could be explained by the molecular orbital confinement theory [53–55]. Hereby, this result also indicated the sensor R6G-TETA was successfully grafted onto the inner surface of SBA-15. We also examined the regeneration of the material after immerge to Cr(III) (20 μM). When the solution was treated with 3 equiv. of EDTA, the quenching fluorescence intensity of SBA-RT almost recovered (Fig. 8). The results indicated

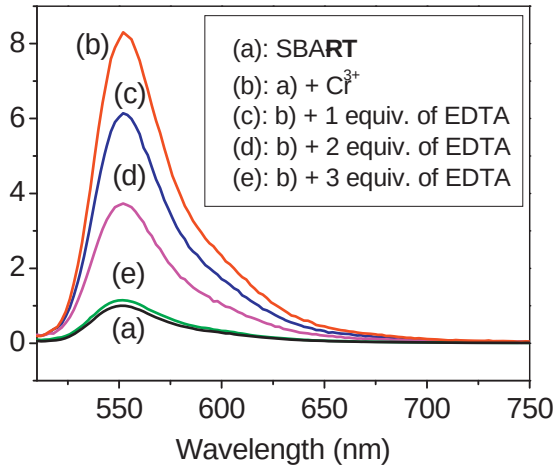

Fig. 8. Regeneration of the Cr(III)-loaded SBA-RT.

that SBA-RT is stable in the whole process, suggesting the potential recyclability.

We then study the stability of the functional material in the practical application process by Low-angle XRD analysis. As shown in Fig. 9, both SBA-15 and SBA-RT exhibited three characteristic diffraction peaks that can be indexed to (100), (110), and (200) diffraction associated with typical two-dimensional hexagonal symmetry (*P6mm*). But the intensities of these characteristic diffraction peaks decreased after grafting of R6G-TETA onto SBA-15. This should be attributed to a reduction in the X-ray scattering contrast between the silica walls and pore-filling material [56–58]. These results demonstrated that the hexagonal arrangement of the mesopore was preserved during the grafting process. Furthermore, the characteristic diffraction peaks of SBA-RT were kept in the process of detection, adsorption and regeneration operation, indicating excellent robustness and stability of the fluorescent material.

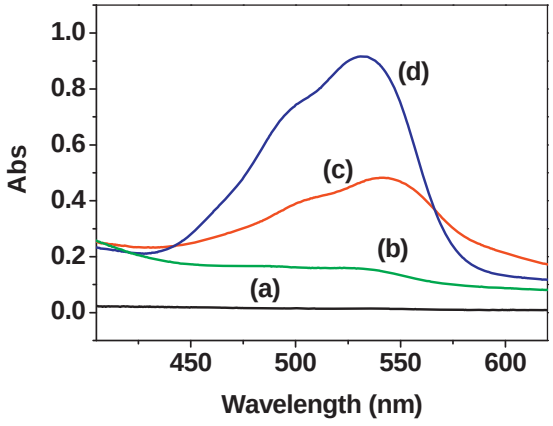

Fig. 7. UV–vis diffuse reflectance spectra of (a) SBA-15, (b) SBA-RT, (c) R6G-TETA + Cr(III) and (d) SBA-RT + Cr (III).

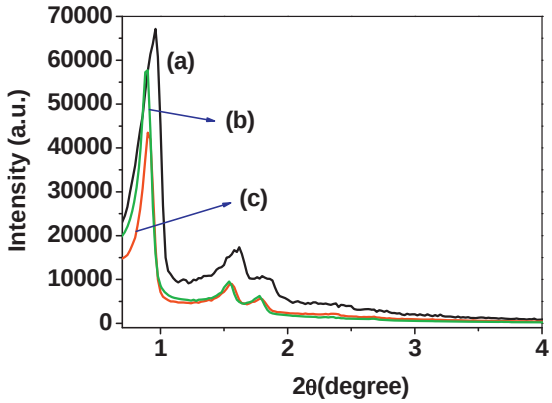

Fig. 9. XRD patterns of (a) SBA-15, (b) SBA-RT and (c) SBA-RT + Cr (III).

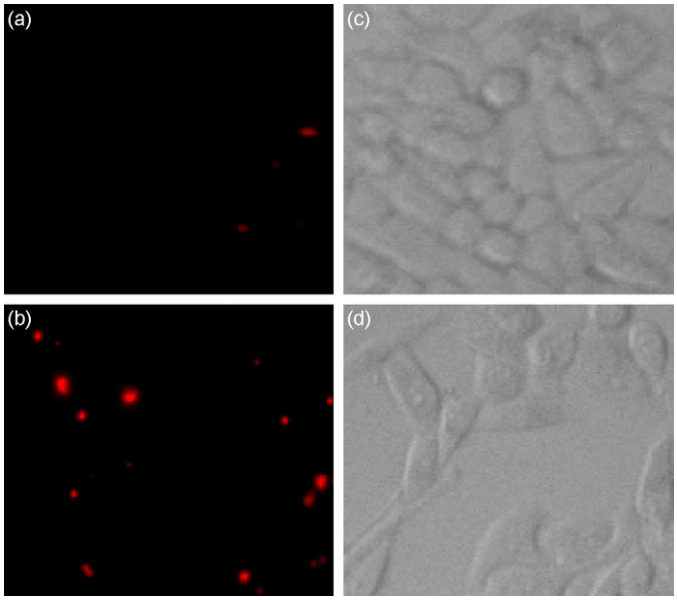

Fig. 10. Fluorescence imaging of SBA-RT induced by intracellular Cr(III). (a) Fluorescence image of HeLa cells incubated with SBA-RT (1 ppm, suspended in PBS medium). (b) Fluorescence image of HeLa cells incubated with SBA-RT, and further incubated with Cr(III) (0.2 mM). (c) and (d) Brightfield image of HeLa cells shown in panel. Excited with green light.

3.3. Fluorescence imaging experiments of SBA-RT in living cells and in vivo

The interactions between surface-functionalized inorganic nanomaterials and animal cells have shown their potential application in biomedicine or biotechnology fields. Recent reports have also shown that mesoporous silica nanomaterials were endocytosed by mammalian cells efficiently [59,60]. The nanomaterial SBA-RT was excited with green light, which is beneficial to cells and tissues of interest, and low background fluorescence is also an advantage. The HeLa cells were incubated with 1 ppm SBA-RT (suspended in PBS medium) for 0.5 h at 37 °C. Then washed with saline three times and mounted on a microscope stage. As shown in Fig. 10(a), the cells displayed weak fluorescence intensity after incubating with SBA-RT, suggesting that the silica material of optimum size was efficiently taken up into cells [61]. In contrast, A "turn-on" of the red fluorescence of HeLa cells were observed by addition of Cr(III) (0.2 mM) into the medium after incubating for another 0.5 h at 37 °C (Fig. 7(b)). The cells were still viable throughout the imaging experiments (Fig. 7(c) and (d)). These experiments indicated that SBA-RT was cell-permeable and could be used to monitor intracellular Cr(III) or study biological processes involving Cr(III) within living cells (Fig. 10).

The successful cell experiments encouraged us to determine if the nanomaterial could be used to detect Cr(III) in living organisms, so *in vivo* detection was evaluated. Five-day-old zebrafish

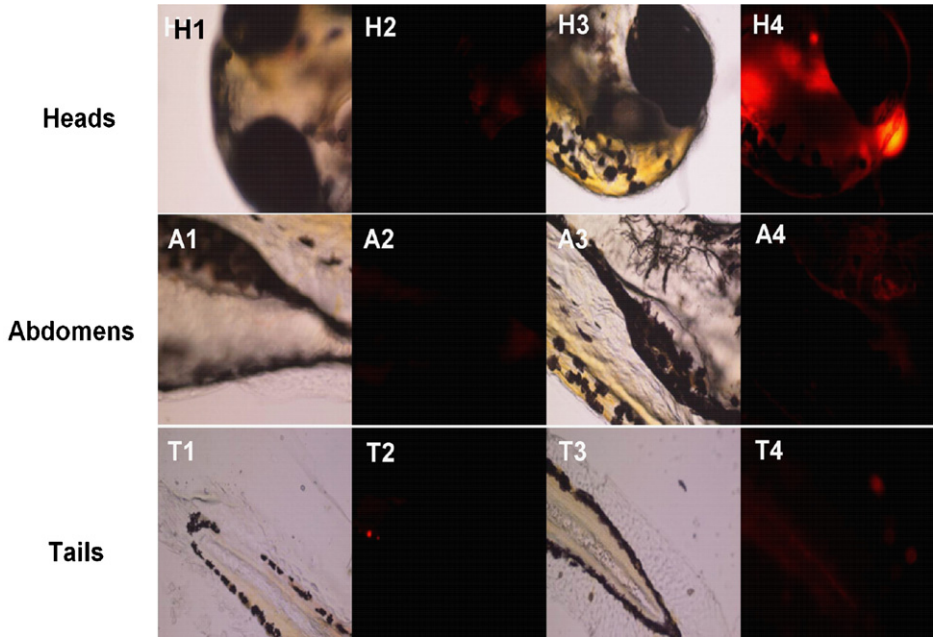

Fig. 11. Fluorescence images of Cr(III) in five day old zebrafish. (H4, A4, T4) Fluorescence image of zebrafish incubated with SBA-RT (4 ppm), and further incubated with Cr(III) (0.2 mM). (H2, A2, T2) Fluorescence image of zebrafish incubated with only SBA-RT. (H1, A1, T1, H3, A3, T3) Brightfield image of zebrafish. Excited with green light.

was incubated with SBA-RT (4 ppm) in PBS media for 0.5 h at 28 °C and washed with saline to remove the remaining silica particles, and then incubated with 0.2 mM Cr(III) for another 0.5 h at 28 °C. After being washed with saline, the zebrafish was imaged by a Nikon eclipse TE2000-5 inverted fluorescence microscopy (excited with green light). As shown in Fig. 11, the functional material was successfully taken up into various parts of the zebrafish and a strong red fluorescence was emerged (Fig. 11, H4, A4, T4), indicating that Cr(III) ions in zebrafish were fluorescently detected by SBA-RT. However, a zebrafish treated with only SBA-RT in the absence of external Cr(III) ions showed a very weak fluorescence signal (Fig. 11, H2, A2, and T2). In particular, the head of the zebrafish exhibited significant luminescent enhancement when it was exposed to external Cr(III). The zebrafish remained alive throughout the imaging experiments. To sum up together, above results implied that the functionalized material should be potentially useful for the study of the toxicity or bioactivity of Cr(III) in living cells and organisms. To best of our knowledge, this is the first fluorescent nanomaterial that can be used to monitor Cr(III) *in vivo*.

4. Conclusions

In conclusion, we have successfully prepared a new functionalized mesoporous material SBA-RT. The hybrid material SBA-RT was not only able to recognize Cr(III) with a highly selective and sensitive by fluorimetric and colorimetric method, but also can remove Cr(III) from water sample. It is stable enough in physiological pH conditions and can be used to study biological processes involving Cr(III) within living cells and living organisms.

Acknowledgment

This work was supported by the National Natural Science Foundation of China.

References

[1] D.Y. Zhao, J.L. Feng, Q.S. Huo, N. Melosh, G.H. Fredrickson, B.F. Chmelka, G.D. Stucky, Science 279 (1998) 548–552.
[2] A.E. Kadib, R. Chimenton, A. Sachse, F. Fajula, A. Galarneau, B. Coq, Angew. Chem. Int. Ed. 48 (2009) 4969–4972.
[3] T.J. Huang, W.X. Tu, Appl. Surf. Sci. 255 (2009) 7672–7678.
[4] V. Polshettiwar, C. Len, A. Fihri, Coord. Chem. Rev. 253 (2009) 2599–2626.
[5] C.F. Jones, D.W. Grainger, Adv. Drug Deliv. Rev. 61 (2009) 438–456.
[6] S. Erbas, A. Gorgulu, M. Kocakusakogullaric, E.U. Akkaya, Chem. Commun. 33 (2009) 4956–4958.
[7] M. Vallet-Regí, F. Balas, D. Arcos, Angew. Chem. Int. Ed. 46 (2007) 7548–7558.
[8] S. Gai, P. Yang, C. Li, W. Wang, Y. Dai, N. Niu, J. Lin, Adv. Funct. Mater. 20 (2010) 1166–1172.
[9] J.M. Rosenholm, E. Peuhu, J.E. Eriksson, C. Sahlgren, M. Lindén, Nano Lett. 9 (2009) 3308–3311.
[10] J.Z. Zhao, M.G. Davidson, M.F. Mahon, G. Kociok-Köhn, T.D. James, J. Am. Chem. Soc. 126 (2004) 16179–16186.
[11] D.P. Ferris, Y. Zhao, N.M. Khashab, H.A. Khatib, J.F. Stoddart, J.I. Zink, J. Am. Chem. Soc. 131 (2009) 1686–1688.
[12] Z.J. Yang, Z. Xie, H. Liu, F. Yan, H.X. Ju, Adv. Funct. Mater. 18 (2008) 3991–3998.
[13] H. Meng, M. Xue, T. Xia, Y.L. Zhao, F. Tamanoi, J.F. Stoddart, J.I. Zink, A.E. Nel, J. Am. Chem. Soc. 132 (2010) 12690–12697.
[14] L. Li, H. Sun, C. Fang, J. Xu, J. Jin, C.J. Yan, Mater. Chem. 17 (2007) 4492–4498.
[15] R. Martínez-Máñez, F. Sancenón, Coord. Chem. Rev. 250 (2006) 3081–3093.
[16] W.S. Han, H.Y. Lee, S.H. Jung, S.J. Lee, J.H. Jung, Chem. Soc. Rev. 38 (2009) 1904–1915.
[17] S. Hudson, J. Cooney, E. Magner, Angew. Chem. Int. Ed. 47 (2008) 8582–8594.
[18] L. Basabe-Desmonts, D.N. Reinhoudt, M. Crego-Calama, Chem. Soc. Rev. 36 (2007) 993–1017.
[19] A. Wada, S. Tamaru, M. Ikeda, I.J. Hamachi, J. Am. Chem. Soc. 131 (2009) 5321–5330.
[20] D.T. Quang, J.S. Kim, Chem. Rev. 110 (2010) 6280–6301.
[21] X.M. Xue, F.T. Li, Micropor. Mesopor. Mater. 116 (2008) 116–122.
[22] B. Lee, Y. Kim, H. Lee, J. Yi, Micropor. Mesopor. Mater. 50 (2001) 77–90.
[23] A.M. Burke, J.P. Hanrahana, D.A. Healyd, J.R. Sodeaud, J.D. Holmesa, M.A. Morris, J. Hazard. Mater. 164 (2009) 229–234.
[24] W. Mertz, K.S. Schwarz, Arch. Biochem. Biophys. 58 (1955) 504–506.
[25] J.C. Chang, L. Gerdom, N.C. Baenziger, H.M. Goff, Inorg. Chem. 22 (1983) 1739–1744.
[26] M. Sarkar, S. Banthia, A. Samanta, Tetrahedron Lett. 47 (2006) 7575–7578.
[27] H. Ksheminska, D. Fedorovych, L. Babyak, D. Yanovych, P. Kaszycki, H. Koloczek, Process Biochem. 40 (2005) 1565–1572.
[28] M. Golonka, Polyhedron 15 (1995) 3667–3689.
[29] P. Raspor, M. Batic, P. Jamnik, D. Josic, R. Milacic, M. Pas, M. Recek, V. Rezic-Dereani, M. Skrt, Acta Microbiol. Immunol. Hung. 47 (2000) 143–149.
[30] M. Zayed, T. Norman, Plant Soil 249 (2003) 139–156.
[31] U.S. Spichiger-Keller, Chemical Sensors and Biosensors for Medical and Biological Applications, Wiley-VCH, 1998.
[32] B. Tang, T. Yue, J. Wu, Y. Dong, Y. Ding, H. Wang, Talanta 64 (2004) 955–960.
[33] M. Royzen, Z. Dai, W.J. Canary, J. Am. Chem. Soc. 127 (2005) 1612–1613.
[34] H.M. Wu, P. Zhou, J. Wang, L. Zhao, C.Y. Duan, New J. Chem. 33 (2009) 653–658.
[35] H.N. Kim, M.H. Lee, H.J. Kim, J.S. Kim, J.Y. Yoon, Chem. Soc. Rev. 37 (2008) 1465–1472.
[36] B.C. Dickinson, C.J. Chang, J. Am. Chem. Soc. 130 (2008) 9638–9639.
[37] A.J. Weerasinghe, C. Schmiesing, E. Sinn, Tetrahedron Lett. 50 (2009) 6407–6410.
[38] K.W. Huang, H. Yang, Z.G. Zhou, M.X. Yu, F.Y. Li, X. Gao, T. Yi, C.H. Huang, Org. Lett. 10 (2008) 2557–2560.
[39] Z.G. Zhou, M.X. Yu, H. Yang, K.W. Huang, F.Y. Li, T. Yi, C.H. Huang, Chem. Commun. 29 (2008) 3387–3389.
[40] J. Mao, Q. He, W.S. Liu, Anal. Bioanal. Chem. 396 (2010) 1197–1203.
[41] J. Mao, L. Wang, W. Dou, X. Tang, Y. Yan, W. Liu, Org. Lett. 9 (2007) 4567–4570.
[42] L. Zhao, S. Wang, Y. Wu, Q. Hou, Y. Wang, S. Jiang, J. Phys. Chem. C 111 (2007) 18387–18391.
[43] M.H. Lee, S.J. Lee, J.H. Jung, H. Lima, J.S. Kim, Tetrahedron 63 (2007) 12087–12092.
[44] A.S.M. Chong, X.S. Zhao, J. Phys. Chem. B 107 (2003) 12650–12657.
[45] Q.T. Meng, X.L. Zhang, C. He, P. Zhou, W.P. Su, C.Y. Duan, Talanta 84 (2011) 53–59.
[46] Q.T. Meng, X.L. Zhang, C. He, G.J. He, P. Zhou, C.Y. Duan, Adv. Funct. Mater. 20 (2010) 1039–1903.
[47] W. Huang, C.X. Song, C. He, G.J. Lv, X.Y. Hu, X. Zhu, C.Y. Duan, Inorg. Chem. 48 (2009) 5061–5072.
[48] Y. Xiang, A. Tong, Org. Lett. 8 (2006) 1549–1552.
[49] National environmental quality standards for surface water, GB 3838-2002, Ministry of Environmental Protection of P.R. China.
[50] C.X. Song, X.L. Zhang, C.Y. Jia, P. Zhou, X. Quan, C.Y. Duan, Talanta 81 (2010) 643–649.
[51] L. Mu, W. Shi, J.C. Chang, S. Lee, Nano Lett. 8 (2008) 104–109.
[52] Y. Yang, K. Yook, J. Tae, J. Am. Chem. Soc. 127 (2005) 16760–16761.
[53] P. Zhou, Q.T. Meng, G.J. He, H.M. Wu, C.Y. Duan, X. Quan, J. Environ. Monit. 11 (2009) 648–653.
[54] W. Xu, H. Guo, D.L. Akins, J. Phys. Chem. B 105 (2001) 1543–1546.
[55] L.Z. Zhang, Y. Xiong, P. Cheng, G. Tang, D. Liao, Chem. Phys. Lett. 358 (2002) 278–283.
[56] B. Marler, U. Oberhagemann, S. Voltmann, H. Gies, Micropor. Mater. 6 (1996) 375–383.
[57] A. Vinu, V. Murugesan, M. Hartmann, J. Phys. Chem. B 108 (2004) 7323–7330.
[58] D. Pérez-Quintanilla, I. Hierro, M. Fajardo, I. Sierra, J. Mater. Chem. 16 (2006) 1757–1764.
[59] S. Giri, B.G. Trewyn, M.P. Stellmaker, V.S.-Y. Lin, Angew. Chem. Int. Ed. 44 (2005) 5038–5044.
[60] C.-Y. Lai, B.G. Trewyn, D.M. Jeftinija, K. Jeftinija, S. Xu, S. Jeftinija, V.S.-Y. Lin, J. Am. Chem. Soc. 125 (2003) 4451–4459.
[61] K. Sarkar, K. Dhara, M. Nandi, P. Roy, A. Bhaumik, P. Banerjee, Adv. Funct. Mater. 19 (2009) 223–234.